Nucleic Acids Research, 2026, **54**, gkag345
https://doi.org/10.1093/nar/gkag345
Chemical Biology and Nucleic Acid Chemistry

Acyclic serinol nucleic acid modification of siRNAs overcomes seed region mediated off-target effects while maintaining potency

Tyler Chickering[1], Joel M. Harp[2], Yongfeng Jiang[1], June Qin[1], Guo He[1], Sarah Hyde[1], Audrey Ihlefeld[1], Maja Janas[1], Derek K. O'Flaherty[1], Sally Schofield[1], John Szeto[1], Christopher S. Theile[1], Klaus Charissé[1], Vasant Jadhav[1], Martin A. Maier[1], Muthiah Manoharan[1], Martin Egli[2], Mark K. Schlegel[1,*]

[1]Alnylam Pharmaceuticals, 675 West Kendall Street, Cambridge, MA 02142, United States
[2]Department of Biochemistry, Vanderbilt University, School of Medicine, Nashville, TN 37232, United States
*To whom correspondence should be addressed. Email: mschlegel@alnylam.com

Abstract

Similar in structure to both glycol nucleic acid (GNA) and peptide nucleic acid (PNA), serinol nucleic acid (SNA) combines the acyclic flexibility of GNA with the amide bond found in PNA and can form stable heteroduplexes with DNA and RNA. While the thermal and metabolic stability of SNA and SNA-modified heteroduplexes has been previously reported, we here describe the application of SNA in RNA interference (RNAi) using GalNAc-conjugated small interfering RNAs (siRNAs). Single incorporations were evaluated at each position across both the guide and passenger strands and subsequently evaluated at key positions in mice. Additionally, the off-target potential of siRNAs containing SNA was assessed. We demonstrate the position-dependent tolerance of SNA inside both the guide and passenger strands, and more specifically, high tolerance of SNA incorporation in the seed region of the guide strand, preserving on-target activity while mitigating microRNA-like off-target effects. Furthermore, the crystal structure of an RNA dodecamer containing a single SNA nucleotide was obtained and the resulting SNA structure was used to explain the activity of SNA containing siRNAs. Thus, SNA constitutes another viable modification in the siRNA toolbox for the development of potent and specific RNAi therapeutics.

Graphical abstract

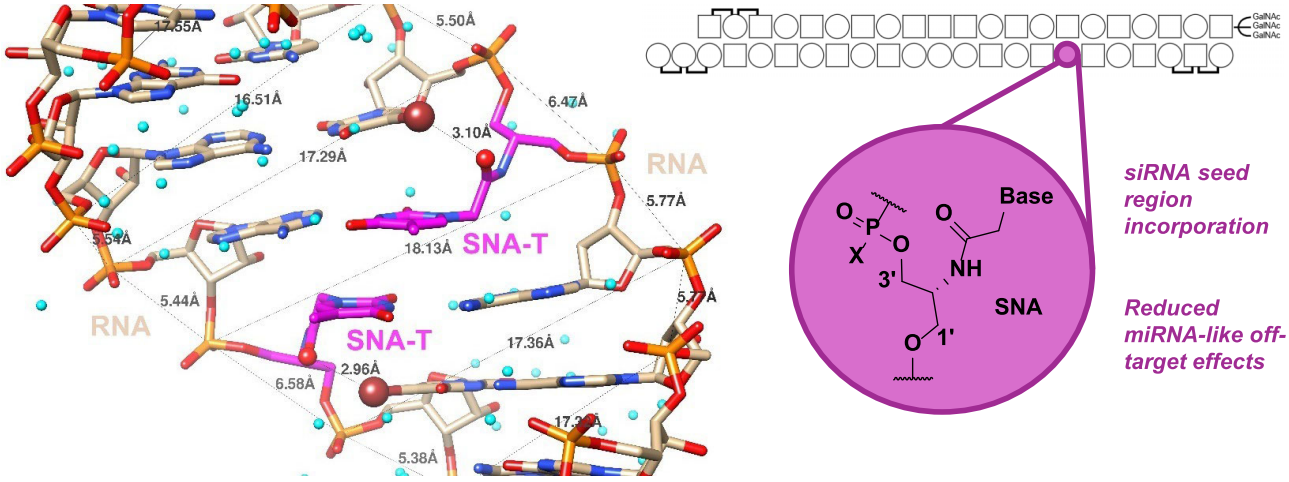

Introduction

RNA interference (RNAi) is the biological process that regulates gene expression via the RNA-induced silencing complex (RISC). The catalytic center of RISC is comprised of Argonaute 2 (Ago2), an endonuclease protein that utilizes 20–25 nucleotide double-stranded small interfering RNA (siRNA)

Received: November 25, 2025. **Revised:** February 25, 2026. **Accepted:** March 22, 2026

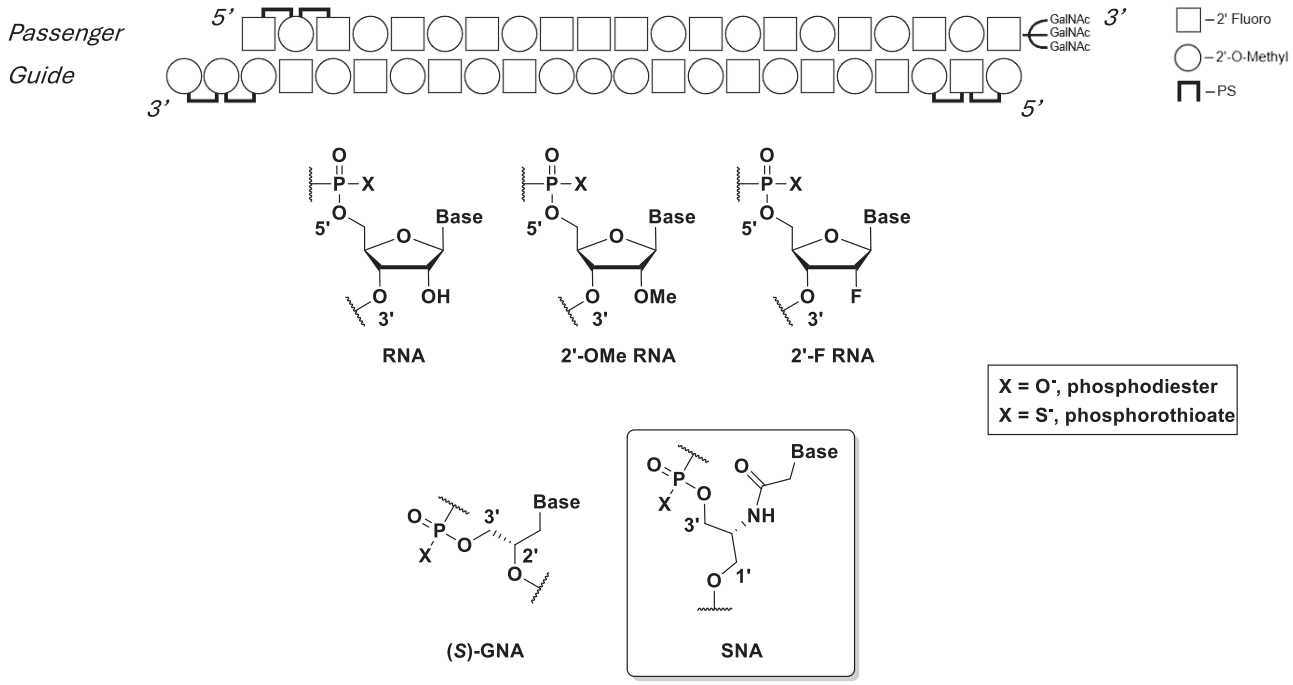

Figure 1. Overview of a GalNAc–siRNA conjugate duplex and the chemical structures of the nucleotides used in this study.

to guide the sequence-specific recognition and cleavage of a target mRNA sequence [1, 2]. Harnessing this natural pathway using rationally designed RNAi-based therapeutics holds tremendous potential by targeting disease-causing protein species at the mRNA level. In fact, RNAi therapeutics have emerged as a new class of medicines that have the potential to treat a wide range of diseases, with eight siRNAs currently approved across several medical agencies around the world for both rare and prevalent diseases [3].

Many years of research directed toward mechanism, chemistry, design, and delivery technologies have enabled and enhanced the therapeutic potential of inherently metabolically unstable and immunostimulatory canonical exogenous RNA. Key chemical modifications of siRNAs have been directed toward improving metabolic stability by preventing enzymatic degradation, mitigating immune stimulation, minimizing off-target effects, and enabling targeted delivery to the cell type of interest [4–8]. For targeted delivery, encapsulation in lipid nanoparticles, trivalent N-acetylgalactosamine (GalNAc), lipophilic, and antibody ligands have been used [4, 5, 9, 10]. Addressing the above challenges through a combination of strategically placed chemical modifications and targeted siRNA delivery was critical for the development of the eight approved RNAi drugs. With regards to improving siRNA specificity, prior work conducted by multiple groups has identified several promising modifications intended for the mitigation of seed-based microRNA (miRNA)-like off-target effects [11] of the siRNA guide strand. These include glycol nucleic acid (GNA), unlocked nucleic acid (UNA), abasic and C3 spacers, threofuranosyl nucleic acid (TNA), 2′-5′-linked RNA, 2′-gem-Me/F RNA, and alkyl phosphonate or amide linkages [12–25]. Notable among these modifications, siRNAs modified with GNA are now a part of a new generation of RNAi therapeutics undergoing clinical trials, and we have reported that the utilization of this approach for the design of ALN–HBV02 (VIR-2218, elebsiran), a GalNAc–siRNA targeted to the hepatitis B virus, resulted in an improved hepatic safety profile in human clinical trials relative to the earlier generation ALN–HBV [21, 26].

To further deconvolute the impact of nucleotide structure on off-target mitigation, and to continue the expansion of chemical modifications in the field, we chose to investigate another acyclic nucleic acid analog in siRNA, serinol nucleic acid (SNA; Fig. 1), as a potentially useful tool for the mitigation of miRNA-like off-target effects. SNA consists of a 2-amino-1,3-propanediol backbone, featuring three carbon atoms between phosphates like natural DNA or RNA [27, 28]. A similar number of bonds between backbone phosphates is featured in other modifications such as UNA, C3-, or abasic-spacers, but contrasts other monomers such as GNA or TNA that feature only two carbon atoms between backbone phosphates. Ramasamy and Seifert first reported the preparation of SNA in 1996, where they incorporated SNA-T into DNA sequences and showed only slightly destabilized cross-pairing with complementary DNA or RNA [27]. Asanuma and colleagues later revisited SNA in greater detail by synthesizing octamers composed solely of SNA and investigated their hybridization properties within SNA homoduplexes or chimeric duplexes with complementary DNA or RNA. Importantly, SNA could efficiently hybridize to form right-handed, A-form like duplex structures with DNA or RNA regardless of the sequence context [29]. Two related homologues, which differ only by the addition of a single methyl group to the C3′ position of SNA, acyclic L- and D-threoninol nucleic acids (L-aTNA and aTNA, respectively), were synthesized in 2001 and 2010 by the Gupta and Asanuma groups, respectively [30, 31]. Whereas both L-aTNA and aTNA have been shown to efficiently self-hybridize, only L-aTNA forms a stable hybrid with DNA or RNA, albeit in a parallel orientation [32]. Despite the small structural differences between SNA, L-aTNA, and aTNA, they demonstrate unique behavior when interacting with canonical nucleic acids [32, 33].

SNA modification of therapeutic oligonucleotides has garnered interest for various antisense approaches such as siRNA, splice-switching oligonucleotides, and antisense-oligonucleotides (ASOs), and studied in detail by the Asanuma group [34–37]. They reported the effect of SNA-modified siRNAs on nuclease stability, on-target activity, and the reduction of passenger strand-driven off-target activity. In these reports, the authors concluded that modification of the siRNA with SNA at terminal positions improved exonuclease resistance relative to canonical RNA. Depending on the placement of the SNA modification in either guide or passenger strand, siRNA activity could be maintained or enhanced. More importantly, SNA modification at both ends of the passenger strand decreased passenger-strand loading-driven off-target effects. In a similar fashion, L-aTNA modification of siRNAs has been shown by the Eritja group to improve nuclease resistance, modulate RNAi activity as a function of position, and influence the interaction of the 3′-overhang with the PAZ domain of Ago2 [38–40]. Most recently, it has been shown that SNA can effectively promote exon-23 skipping of the mouse dystrophin gene transcript in *mdx* myotubes, and that gapmer ASOs modified with SNA can induce efficient gene silencing in mouse kidney, similar to that of 2′-O-methoxyethyl (2′-MOE) gapmers, but with an improved duration and safety profile [34, 36], further reinforcing the utility of SNA as a useful modification across therapeutic oligonucleotide modalities.

Due to its simpler structure, and a potentially more favorable antiparallel pairing to RNA, we chose to further investigate SNA as an interesting acyclic structural modification for the mitigation of seed-mediated, miRNA-like off-targets of siRNAs. Herein, we report a detailed investigation into the impact of SNA modification on the thermal stability, on-target activity, and seed-mediated miRNA-like off-target activity of GalNAc-conjugated siRNAs. Because homopolymers of SNA were shown to be incompatible with RNAi [37], we investigated singly modified guide or passenger strands. We compared the SNA-mediated impact on thermal stability to those values reported for duplexes containing GNA modification at identical positions. We determined the X-ray crystal structure of an RNA dodecamer duplex with a single SNA-T per strand. To assess the effect of SNA modification on *in vitro* RNAi activity, we performed a walk of a single SNA residue along the passenger and guide strands of a GalNAc–siRNA targeted against mouse transthyretin (*Ttr*). We demonstrated using subcutaneous injections in mice that the favorable potency of the SNA-modified anti-*Ttr* GalNAc–siRNA observed *in vitro* is also maintained *in vivo*. Finally, we show that SNA modification in the seed region, most prominently when incorporated at position 7 of the guide strand, can mitigate miRNA-like off-target effects in a dual-luciferase reporter system.

Materials and methods

Oligonucleotide synthesis

All oligonucleotides were synthesized on a MerMade 192 or MerMade 12 synthesizer according to previously published protocols [20, 22]. 2′-O-methyl (2′-OMe) and 2′-deoxy-2′-fluoro (2′-F) phosphoramidites were purchased commercially. SNA phosphoramidites were synthesized according to previously published protocols [27–29] and dissolved in acetonitrile at a concentration of 100 mM for coupling using the same conditions as those used for 2′-OMe and 2′-F. The identity and purity of all oligonucleotides in these studies were confirmed using ESI–LC/MS and IEX HPLC, respectively.

Thermal melting experiments

Melting studies were performed in 1 cm path length quartz cells on a Cary 300 UV-visible spectrophotometer equipped with a Peltier temperature-controlled multicell holder. Each cuvette contained 800 μl of sample solution covered by 200 μl of light mineral oil. Samples were first annealed in the instrument by heating at a rate of 5°C/min from 25°C–95°C followed by cooling at the same rate from 95°C–25°C. After a waiting period of 3 min, melting curves were monitored at 260 nm with a heating rate of 1°C/min from 25°C–95°C. Melting temperatures (T_M) were calculated from the first derivatives of the heating curves and the reported values are the result of at least two independent measurements.

Crystallization, data collection, and refinement

Crystals of 5′-CGCGAA(T)(Br5U)CGCG-3′ were grown by sitting-drop vapor diffusion. Drops contained 400 nl of 1 mM RNA and 400 nl of buffer containing 10% 2-methyl-2,4-pentanediol (MPD), 12 mM spermine 4 HCl, 80 mM potassium chloride, and 40 mM sodium cacodylate (pH 6.0). Drops were equilibrated against reservoirs containing 70 μl of 40% MPD at 20°C. Crystals were harvested directly from the drop using Mitegen™ microloops and flash-cooled by plunging into liquid nitrogen. A Br-SAD dataset was collected using synchrotron radiation at 0.9184 Å wavelength on beamline 21-ID-D of the Life Sciences-Collaborative Access Team at the Advanced Photon Source at Argonne National Laboratory. Diffraction data were processed using xia2 and DIALS [41, 42]. Phasing of the data was done using HKL2MAP graphical interface to SHELXC, SHELXD, and SHELXE [43–45]. Model building was done manually using COOT [46]. Refinement was done using PHENIX. Due to the limitation of the single rotation axis, the synchrotron dataset showed low completeness in the low-resolution bins. A fresh crystal was used to collect a complete dataset in-house at the Vanderbilt University Center for Structural Biology Biomolecular Crystallography Facility using a Bruker D8 Venture (Bruker AXS, Madison, WI) system. The system includes an Excillum D2 + MetalJet X-ray source operated at 250W with Helios MX optics providing Ga Kα radiation at 1.3418 Å wavelength. The crystal was mounted on a kappa axis goniometer and maintained at 100K using an Oxford Cryosystems Cryostream 800 cryostat. The detector was a PHOTON III C14 charge-integrating pixel array detector. Data collection was performed in shutterless mode. Diffraction data were reduced using Proteum5 software (Bruker AXS, Madison, WI). The in-house data were phased by molecular replacement using the Br-SAD structure. Refinement and preparation for deposition was done using the Phenix suite [47]. Selected crystal data, data collection, and refinement parameters are summarized in Supplementary Table S5.

In vitro screening

Primary hepatocytes were obtained from Gibco and cultured in Williams E Medium (Gibco) with 10% fetal bovine serum. Cells were plated in 384 well plates at a density of 5000 cells per well on collagen-coated plates, and siRNA was added to

a final concentration of 10 or 0.1 nM. Transfection of siRNA (5 μl) was accomplished in 40 μl complete medium containing 4.9 μl OptiMem I (Gibco) and 0.1 μl RNAiMax (Invitrogen). At 24 h after transfection, RNA extraction was performed using Dynabeads (Inivtrogen), followed by reverse transcription according to the manufacturer's protocols (ABI, High Capacity). Mouse *Ttr* was quantified by RT-qPCR (Applied Biosystems, #Mm00443267_m1), with mouse *Gapdh* (4352339E) as loading control. Relative levels of *Ttr* were determined by normalizing to *Gapdh* RNA expression from the same sample, and these values were subsequently expressed as percent of a mock control. All data points are the average of four measurements.

In vitro screening in the dual-luciferase reporter assay

COS-7 cells were cultured at 37°C and 5% CO_2 in Dulbecco's modified Eagle medium supplemented with 10% fetal bovine serum. Cells were cotransfected in 96-well plates (15 000 cells/well) with 10 ng luciferase reporter plasmid and 0.64 pM to 50 nM siRNA in five-fold dilutions using 2 g/ml Lipofectamine 2000 (Thermo Fisher Scientific) according to the manufacturer's instructions. Cells were harvested at 48 h after transfection for the dual luciferase assay (Promega) according to the manufacturer's instructions. The reporter plasmids were generated by cloning targeting sequences into the psiCHECK2 vector between Xho1 and Not1 restriction sites. The on-target reporter plasmid contained a single site with perfect complementarity to the guide strand in the 3′-UTR of Renilla luciferase. The off-target reporter plasmid contained four tandem seed complementary sites separated by a 19-nucleotide spacer (5′-TAATATTACATAAATAAAA-3′) in the 3′-UTR of renilla luciferase. Both plasmids co-expressed firefly luciferase as a transfection control. The specific insert sequences were as follows:

Ttr on-target: ATAAACAAGGTTTGACATCAATCTAGC TATATCTTTAAGAATGATAAACT **AAACAGTGTTCTTGCTCTATAA**GACATTGGTGAGGA AAAATCCTTTGGCCGTTTCCAAGAT CTGACAGTGCA

Ttr off-target: ATAAACAAGGTTTGACATCAATCTAGC TATATCTTTAAGAATGATAAACT **GCTCTATAA** TAATATTACATAAATAAAA**GCTCTATAA**TAATATTACAT AAATAAAA**GCTCTATAA**T AATATTACATAAATAAAA **GCTCTATAA** GACATTGGTGAGGAAAAATCCTTTG GCCGTTTCCAAGATCTGACAGTGCA

Care and use of laboratory animals

All studies were conducted by certified laboratory personnel using protocols consistent with local, state and federal regulations, as applicable, and experimental protocols were approved by the Institutional Animal Care and Use Committee at Alnylam Pharmaceuticals. All animals were acclimated in-house for 48 h prior to study start.

In vivo screening, serum protein quantification, liver mRNA quantification, and liver siRNA quantification in mice

Female C57BL/6 mice ∼6–8 weeks of age were obtained from Charles River Laboratories and randomly assigned to each group. All dosing solutions were stored at 4°C until 1 h before the time of injection, when they were removed from storage and allowed to reach room temperature. Animals received a single subscapular subcutaneous injection of siRNA or 1× PBS at the indicated dose, prepared as an injection volume of 10 μl/g in 1× PBS. At the indicated time pre- or post-dosing, blood was collected via retroorbital bleed. Serum samples were kept at room temperature for 1 h and then spun in a microcentrifuge at 21 000 × *g* at room temperature for 10 min and subsequently stored at −80°C until analysis. TTR serum protein levels were measured by ELISA (serum was diluted 1:4000 and used in a mouse prealbumin kit according to the manufacturer's instructions (ALPCO, 41-PALMS-E01). Animals were sacrificed at the days indicated in the figures, after which livers were harvested and snap frozen for further analysis.

For the extraction of RNA, powdered liver (∼10 mg) was resuspended in 500 μl QIAzol and a 5-mm steel grinding ball was added to each sample. Samples were homogenized at 25/s for 2 × 5 min at 4°C using a TissueLyser LT (Qiagen). Samples were incubated at room temperature for 5 min followed by addition of 100 μl chloroform. Samples were mixed by vigorously shaking the tubes, followed by a 10-min incubation at room temperature. Samples were spun at 12 000 × *g* for 15 min at 4°C and the supernatant was removed to a new tube and 1.5 volumes of 100% ethanol was added. Samples were then purified using an RNeasy Kit (Qiagen). Samples were eluted from RNeasy columns with 60 μl RNase-free water (Ambion) and quantified on a NanoDrop (Thermo Fisher Scientific). 1.5 μg of RNA was used to generate cDNA using a High-Capacity cDNA Reverse Transcription Kit (Applied Biosystems, 4368813). qPCR reactions were performed using gene-specific TaqMan assays for each target (Thermo Fisher, Mm00443267_m1 for *Ttr* and Mm00439249_m1 for *Hao1*) and mouse *Gapdh* as an endogenous control (Thermo Fisher, 4352339E). Real-time PCR was performed in a Roche LightCycler 480 using LightCycler 480 Probes Master Mix (Roche, 04707494001). Data were analyzed using the ΔΔCt method normalizing to control animals dosed with PBS alone.

Mass identification of siRNA metabolites in mouse liver

Mice were sacrificed 7 days post dose of the indicated GalNAc–siRNAs and the livers were snap frozen in liquid nitrogen and ground into powder for analysis. Lyophilized mouse liver (50 mg) was thawed at RT to which 430 μl proteinase K digestion buffer [105 mM Tris–HCl, 17.5% tween 20%, 1.26% triton X-100, 50 mM $CaCl_2$, 3 mM disodium ethylenediaminetetraacetic acid (EDTA), pH 8.0] was added. After briefly vortexing (20 s) and sonicating (10 min) at RT using a bath sonicator, 20 μl proteinase K (600 mAU/ml; Qiagen, Cat. 19133) was added and vortexed (5 s). Samples were centrifuged at 12 700 RPM for 10 min and three aliquots of 100 μl supernatant was removed. To each fraction, 900 μl lysis loading buffer (Phenomenex, Cal. ALO-8579; adjusted to pH 5.5 with citric acid) with 0.5 ng/ml internal standard (12 nucleotide fully modified 2′-O-methyl uridine oligonucleotide) was added. Solid phase extraction (SPE) was facilitated by an automated positive pressure manifold (Biotage, Extrahera) and Clarity OTX plates (Phenomenex, Cat. 8E-S103-EGA) per manufacturer's recommendations. Briefly, the SPE plate was conditioned with 1 ml methanol and washed with 1.9 ml buffer (50 mM ammonium acetate, 2 mM sodium azide; pH 5.5). Samples were loaded (1 ml), washed 3× with 1.5 ml wash buffer (50 mM ammonium acetate in 50:40:10

H_2O:MeCN:THF; pH 5.5), and eluted with 600 µl elution buffer (10 mM EDTA, 10 mM DTT (dithiothreitol), 100 mM ammonium bicarbonate, 50:40:10 H_2O:MeCN:THF; pH 8.8). Solvent was evaporated to dryness using a nitrogen manifold (Biotage, Turbovap) at 40°C and 65 psi. Samples were reconstituted in 40 µl LC–MS grade water. Three replicate samples were combined and 30 µl was analyzed via high accuracy high resolution mass spectrometry (Thermo Scientific, QExactive) coupled to an Ultimate 3000 UPLC (Dionex). Chromatography was performed with a XBridge BEH XP C_8 column (130 Å, 2.5 µm, 2.1 × 30 mm; Waters) at 80°C and a linear gradient of methanol (1%–35%) in mobile phase A (16 mM triethylamine, 200 mM 1,1,1,3,3,3-hexafluoro-2-propanol in water). The mass spectrometer was equipped with a HESI II source and operated in negative ion full scan mode with a scan range of 500–2000 m/z at a resolution setting of 35 000. Spray voltage was 2.8 kV, auxiliary gas and capillary temperature were set to 300°C. Data analysis and signal deconvolution were performed using XCalibur software (Thermo Scientific) interfaced to Promass HR (Novatia LLC).

Modeling

Coordinates for the crystal structure of the complex between human Ago2 and miR-20a (PDB ID code 4f3t [48]), the Ago2 seed complex with guide and passenger siRNA bound (PDB ID code 4w5t [11]), and Ago2 with miR-122 bound to a seed and supplementary paired target (PDB ID code 6n40 [49]) were downloaded from the Protein Data Bank (http://www.rcsb.org). Using the program UCSF Chimera [50], individual RNA nucleotides at positions g1, g2, g3, g5, g6, and g7 in the miR-20a complex were substituted by SNA-T from the crystal structure of the modified RNA duplex. Similarly, the RNA nucleotide at position g13 in the Ago2 complex with seed and supplementary region paired, and nucleotides at positions g20 and g21 (g22 and g23, respectively, of si-1) bound to the PAZ domain in the Ago2 seed complex were replaced by SNA-T. All models were energy-minimized with Amber 14 [51] as implemented in UCSF Chimera until convergence was reached.

Results

Thermal stability of RNA and GalNAc–siRNA duplexes containing SNA

An initial evaluation of duplex thermal stability was performed using a model 12-mer RNA duplex modified at an internal position with SNA. A single SNA modification destabilized the RNA duplex thermal melting (T_M) by a range of −9°C to −13°C (Supplementary Table S1), consistent with a previous report on the stability of a DNA/RNA heteroduplex containing a central SNA modification [27]. The average destabilization for a single SNA modification in RNA of −10.4°C is almost identical to the reported value of −10.3°C for (*S*)-GNA, however, the incorporation of SNA-C or SNA-G (−12.6°C or −9.7°C, respectively) was less disruptive than the corresponding incorporation of GNA-C or GNA-G (−16.8°C or −12.1°C, respectively) in the same RNA sequence context [20]. On the other hand, the incorporation of SNA-A or SNA-T resulted in a more pronounced decrease in thermal stability (−8.8°C or −10.5°C, respectively) than that reported for GNA-A or GNA-T incorporation (−7.7°C or −4.7°C, respectively).

To enable an assessment of the impact of SNA modification on both duplex thermal stability and inherent potency, a well-characterized GalNAc–siRNA targeting mouse *Ttr* was chosen (si-1; Supplementary Table S2, [4]). Single SNA nucleotides were inserted at every possible position of the GalNAc–siRNA duplex (Supplementary Table S2). Profiles revealed a general SNA-mediated decrease in thermal stability that was dependent on both the position of modification and nucleobase identity (Fig. 2A and Supplementary Table S3). In general, the magnitude of the effect increased as the SNA modification moved more toward the center of the duplex. Figure 2B shows that the average destabilization of SNA-A and -T modification at internal positions was −4.2°C and −5.0°C, respectively, which was slightly higher than that of GNA-A and -T modification (−2.9°C and −3.9°C, respectively; see [20]). Notably, modification of positions 8, 9, 12, 15, or 17 on the guide strand (g8, g9, g12, g15, or g17) with SNA was found to be the most destabilizing and correlated in each instance to modification of a C or G nucleobase. A similar tendency was observed for modification of positions 7, 10, 13, 14, or 16 on the passenger strand (p7, p10, p13, p14, or p16; Supplementary Fig. S1). The trend of increased thermal destabilization with SNA-C or SNA-G (−6.9°C and −6.3°C, respectively) was consistent with, but less pronounced than that of GNA-C or GNA-G (−8.2°C and −6.8°C, respectively), presumably due to the nature of the rotated base-pairing featured in all GNA nucleotides, making it refractory to hybridization with G/C-rich RNA [22]. Overall, the SNA-mediated effect on T_M ranged from +0.1 to −8.1°C, which was very similar to the range observed with GNA in the same GalNAc–siRNA (+1.1 to −9.8°C).

Crystal structure of an SNA-modified RNA dodecamer

A total of seven different self-complementary RNA octamers or dodecamers containing a single SNA thymidine, additionally modified with either 5-bromouridine or 5-bromocytidine to support anomalous phasing, were subjected to crystallization trials (see Supplementary Table S4). Multiple conditions in a sparse matrix crystallization screen yielded crystals for the dodecamer 5′-CGCGAA(T)(Br5U)CGCG-3′, with (T) and (Br5U) representing a SNA-T and 5-bromouridine nucleotide, respectively (sequence x-5, Supplementary Table S4). Crystals diffracted to 1.6 Å resolution and the structure was phased by Br-SAD. They belonged to space group *P*1 with unit cell constants 24.02 Å, 29.19 Å, 29.78 Å, 110.9°, 100.3°, 111.6° and contain a single duplex. Due to the constraints of a single rotation axis and *P*1 space group, low-resolution data were not complete. Another crystal was used to collect fully complete diffraction data in-house as described in the "Materials and methods" section. Data collection, phasing, and refinement parameters are summarized in Supplementary Table S5.

The modified RNA adopts a so-called A' conformation whose hallmarks include reduced inclination of base pairs (∼10°), increased helical rise (∼3 Å), and a wider major groove (∼8 Å) compared to a standard A-from RNA duplex. Structural comparisons between the SNA-modified RNA and the parent 12-mer as well as an A'-form duplex are shown in Supplementary Fig. S2. The presence of SNA residues has both consequences for the overall conformation of the RNA duplex and results in significant local conformational changes. SNA features four bonds between backbone and base (C2′—NH—

A

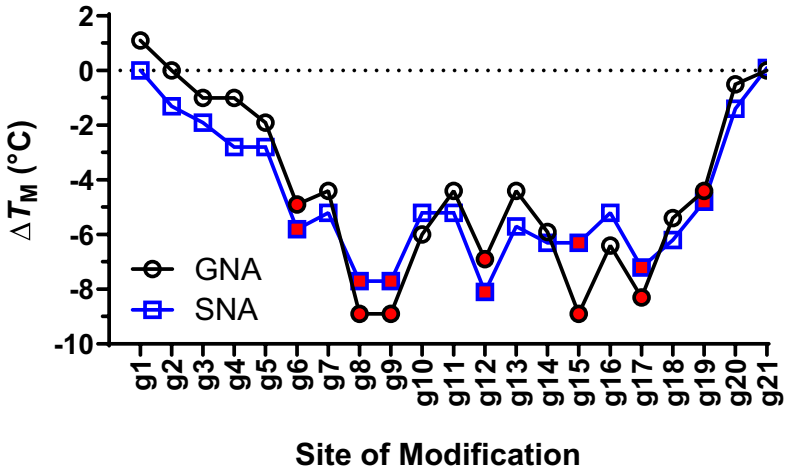

B

Modification	ΔT_m (°C) [a]	Range [b]
Single SNA substitution	-5.4 ± 1.8	+0.1 to -8.1
A	-4.2 ± 1.8	0.0 to -6.3
C	-6.9 ± 1.1	-4.8 to -8.1
G	-6.3 ± 1.2	-4.8 to -8.1
T	-5.0 ± 1.7	+0.1 to -7.6

[a] Each reported value is the average of two independent measurements at a duplex concentration of 1 μM in 0.25x PBS buffer. The values represent the average impact of single substitution from positions 3-19 across either guide or passenger strand of the conjugate duplex. [b] Specific ranges cover all positions of the 21/23-mer siRNA-GalNAc conjugate duplex

Figure 2. Effect of SNA substitution on GalNAc–siRNA duplex thermal stability ($n = 2$). (**A**) T_M values relative to parent GalNAc–siRNA (si-1) with guide strands modified with SNA or GNA (data from [20]) at the specified position. Positions with a C or G nucleobase are indicated by the red squares or circles. (**B**) Average effect of single SNA substitution on GalNAc–siRNA duplex thermal stability.

C(O)—CH_2—N1[T]) compared to just three in RNA (C3′—C2′—C1′—N1[U]) or (C4′—O4′—C1′—N1[U]). Because the Watson–Crick pairing type is maintained between SNA-T and RNA-A, the inter-strand phosphate–phosphate spacing increases by ∼1 Å to >18 Å at SNA incorporation sites (Fig. 3A) compared to the rest of the duplex. Like with RNA, the SNA backbone contains six bonds, but the torsion angles of SNA-T nucleotides differ distinctly from those in RNA (Fig. 3A). In SNA, three of the angles (β, γ, and ϵ) fall into the *ap* and the others in the *sc*- range. By comparison, for adjacent RNA nucleotides, only β and ϵ adopt an *ap* conformation and all others are in the *sc*+ or *sc*− ranges. These differences result in intra-strand phosphate-phosphate distances for SNA residues (6.47 and 6.58 Å) that are reminiscent of B-form DNA and ∼1 Å longer than those observed in neighboring RNA nucleotides (ca. 5.5 Å on average). In both strands the carbonyl oxygen of the SNA amide linker is engaged in a halogen bond to the bromine at C5 of the 3′-adjacent RNA-U (distances of 3.10 Å in strand 1 and 2.96 Å in strand 2; Fig. 3A). It is likely that these interactions help to stabilize the SNA-modified RNA duplex, but we don't believe that they should be viewed as an artifact of bromine modification. Thus, in the absence of bromine, SNA could be stabilized by [n] C = O … H-C5(Py) [$n + 1$] and [n] C = O … H-C8(Pu) [$n + 1$] interactions. It is conceivable that such H-bonds will have a length of ∼3.5 Å, assuming that the amide moiety can tilt slightly toward the base of the following residue (Fig. 3A). We grew crystals of an SNA-modified RNA 12-mer without bromine and of another 12-mer with bromine at an alternative location (sequences x-7 and x-8, respectively, Supplementary Table S4). Neither of the crystals belonged to space group *P*1 and they diffracted to <2.5 Å resolution. Phasing of the structure from x-7 using molecular replacement and the refined structure of the modified RNA as a model did not yield a solution. The anomalous signal in the data collected for x-8 was insufficient for solving the structure by Br-SAD.

An additional conformational change observed in the SNA-modified RNA duplex concerns local unwinding. The central region of the modified duplex viewed along the stacking direction demonstrates a negative twist between SNA-T and RNA-A preceding it in both strands (Fig. 3B). The resultant twist between that RNA-A and the RNA-U after SNA-T is only 26°, and the unwinding thus amounts to −40° relative to the expected twist over two base-pair steps in canonical A-form RNA (66°). Considering all these conformational differences, one is tempted to view SNA as a poor mimic of a

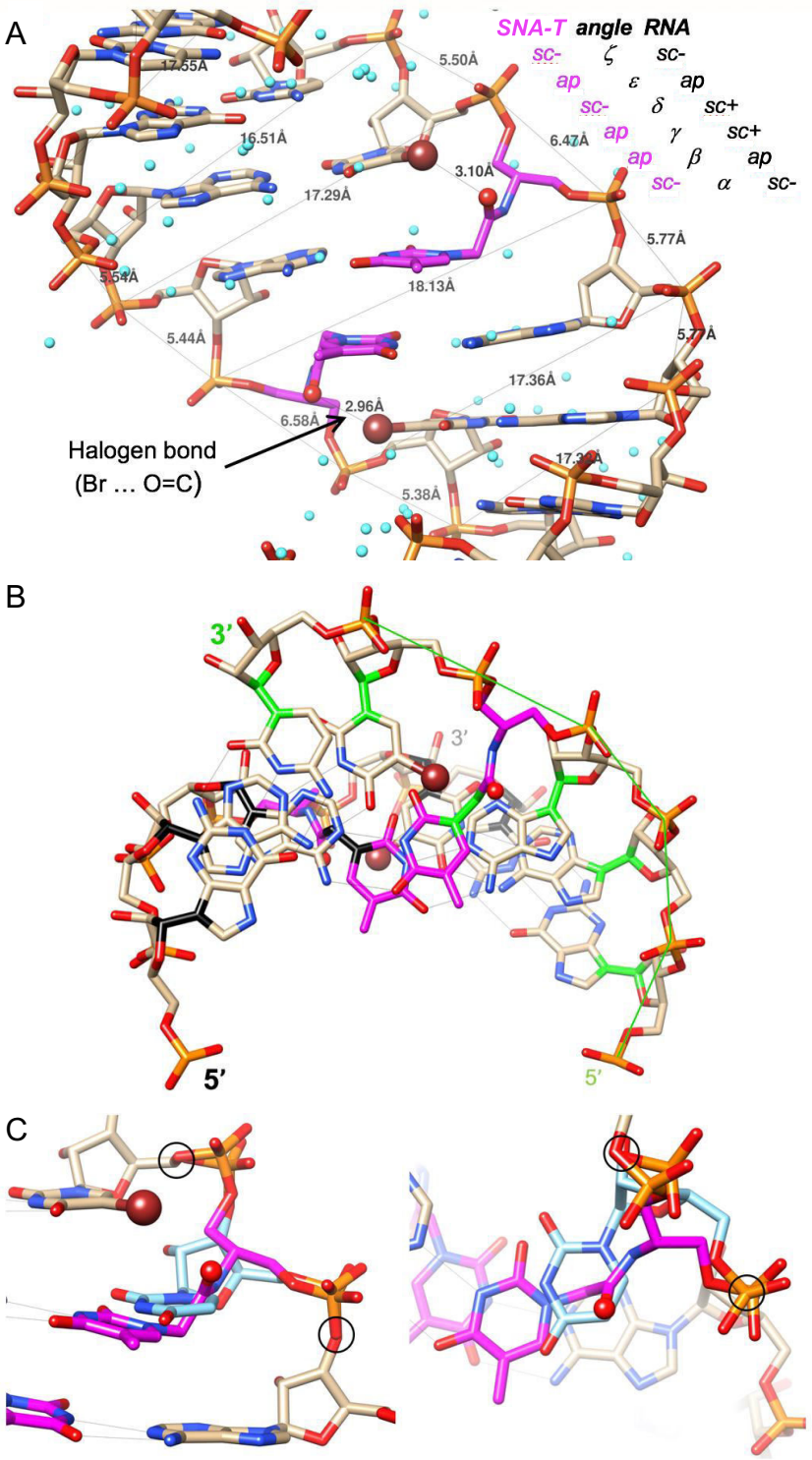

Figure 3. Crystal structure of an SNA-modified RNA duplex and conformational consequences of SNA modification. (**A**) View into the relatively wide major groove of the A′-form RNA duplex. Carbon, oxygen, nitrogen, phosphorus, and bromine atoms of RNA nucleotides are colored in tan, red, blue, orange, and maroon, respectively, and carbon atoms of SNA-T nucleotides are highlighted in magenta. Water molecules are small cyan spheres. Inter- and intra-strand phosphate-phosphate and C = O … Br halogen bond distances are indicated with thin solid lines. Backbone torsion angle ranges for RNA and SNA are shown at the upper right. (**B**) View down the central stack of base pairs, demonstrating the negative helical twist of ca. −10° between SNA-T and the preceding A in both strands. Glycosidic bonds are highlighted in green in one strand and black in the other. (**C**) Overlay of SNA-T (magenta carbon atoms) and RNA-U (light blue carbon atoms) viewed into the major groove (left) and along the stacking direction (right), demonstrating significantly different orientations of the nucleobases inside an RNA duplex. Circles highlight continuity of the backbone on the 5′- and 3′- sides of the insertion site despite deviating orientations of phosphates.

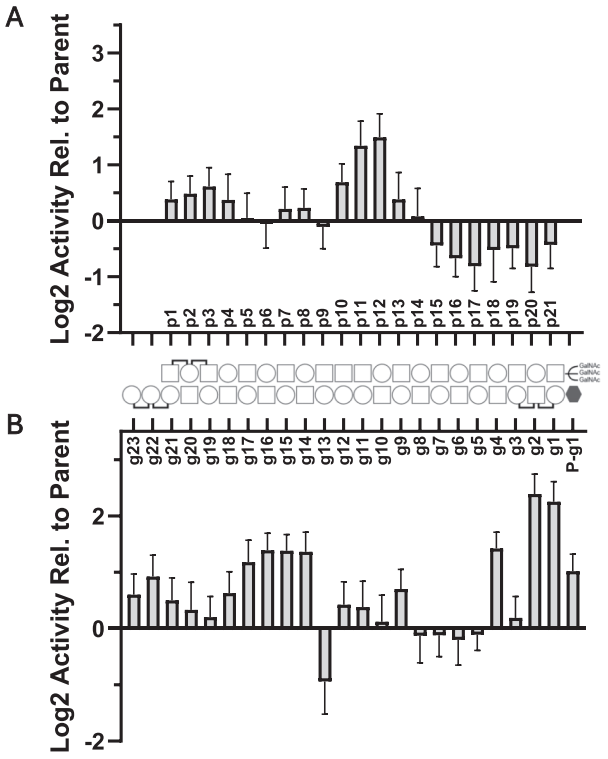

Figure 4. Relative *in vitro* activity of GalNAc–siRNAs transfected at a dose of 10 nM in primary mouse hepatocytes modified using a single SNA nucleotide at each position of either the passenger (**A**) or guide (**B**) strand ($n = 4$). The logo of the GalNAc–siRNA is shown for clarity, and the parent modification pattern is as indicated in Fig. 1. A 5′-phosphate is indicated by the black hexagon and was only included in the indicated GalNAc–siRNA (P-g1, or si-3). Relative $\log_2$ activity [$\log_2$(SNA-modified siRNA) − $\log_2$(parent)] of <0 indicates an improved activity over the parent whereas a value of >0 indicates a loss of activity relative to the parent.

double-helical RNA conformation. This impression is also supported by an overlay of RNA-U and SNA-T that reveals significantly different orientations inside an RNA duplex (Fig. 3C) and was consistent with the destabilization observed with modified strands in UV melting experiments.

In vitro gene silencing of modified siRNA containing SNA modifications

We chose to investigate the effect of SNA modification on RNAi activity within a fully modified GalNAc–siRNA construct targeting the rodent *Ttr* gene. The parent sequence (si-1), fully modified with 2′-OMe, 2′-F, and site-specific phosphorothioate backbone modifications, was previously designed to provide optimal productive association with Ago2 while resisting nucleolytic degradation [4]. The SNA-containing GalNAc–siRNAs (Supplementary Table S2) were first screened for activity in primary mouse hepatocytes via transfection at two dose levels (10 and 0.1 nM). We observed a position-dependent tolerance of SNA modification in both the passenger and guide strand of the tested GalNAc–siRNA. Certain positions such as g1, g2, g4, and g14-17 of the guide, and p11-12 of the passenger were detrimental to RNAi activity relative to the parent sequence (Fig. 4, Supplementary Figs S3and S4, and Supplementary Table S6). Activity could be partially restored to the siRNA modified at g1 by chemically installing a 5′-monophosphate, suggesting a lack of kinase activity directly on the terminal SNA nucleotide. It is perhaps unsurprising that positions g2, g14, p11, and p12 were sensitive to SNA modification, as these have all been reported to be sterically constrained (g2, g14), or crucial for passenger slicing and removal (p11, p12). It was also interesting to observe that modification with SNA was not tolerated in the region adjacent to and including the supplemental region of the guide strand (g14–17), suggesting potential challenges with reaching a stable "two-duplex" state just prior to the fully paired conformation to support target catalysis [52]. Improved activity was notable when SNA was incorporated at p15–p21, perhaps because of an effect on thermal rebalancing of the duplex for optimal RISC loading of the desired guide strand. Most importantly, activity was maintained relative to the parent for modification at g5–g8, positions that have been previously demonstrated to be critical for modulating miRNA-like off-target behavior of siRNAs.

Analysis of miRNA-like off-target activity in a luciferase reporter assay

Encouraged by the fact that siRNA activity was well maintained when a single SNA modification was incorporated at positions g5–g8 in the seed region, we wanted to evaluate the potential of SNA modification to mitigate off-target activity in a dual-luciferase reporter assay. We chose the same *Ttr*-targeting siRNA sequence used for the single nucleotide SNA walk but updated the chemical modification pattern to be consistent with that of our more advanced designs for maximal potency and duration in eventual rodent studies (Supplementary Table S7; see [8, 21]). This GalNAc–siRNA was also chosen because it has shown robust miRNA-like off-target behavior, resulting in a strong signal in the dual-luciferase off-target reporter assay, substantial transcriptome dysregulation in RNA sequencing of treated hepatocytes, and toxicity in rats when administered at supratherapeutic doses [21].

SNA incorporation in this more advanced GalNAc–siRNA design (si-48, si-49, si-50, si-51) resulted in a change in T_M relative to parent (si-47) that was consistent to within 1°C of the changes observed in the analogous siRNAs used in the single nucleotide walk (Supplementary Tables S3 and S7). To determine whether the measured T_M values for these fully modified GalNAc–siRNA duplexes could reflect the differences in hybridization expected with the target mRNA, we determined the melting temperature of hybrid duplexes consisting of the modified guide strands of these GalNAc–siRNAs with a complementary RNA of either 23 nucleotides in length (fully complementary) or 33 nucleotides in length (fully complementary with 5 nucleotide overhangs). Although the absolute T_M values decreased by ∼9°C–13°C for the duplexes with 23-mer RNA and ∼10°C–15°C for the 33-mer RNA, the relative changes in magnitude of T_M due to SNA incorporation were highly correlated with those of the fully modified GalNAc–siRNAs (Supplementary Tables S7 and S8, and Supplementary Fig. S5). There was also a strong correlation between the T_M data generated for duplexes with a 23-mer or 33-mer RNA complement (Supplementary Fig. S6). The cumulative data suggests that T_M measurement of fully modified GalNAc–siRNA serves as a good predictor of the relative impact of chemical modification on the thermal stability of a guide strand complexed with the targeted mRNA.

A

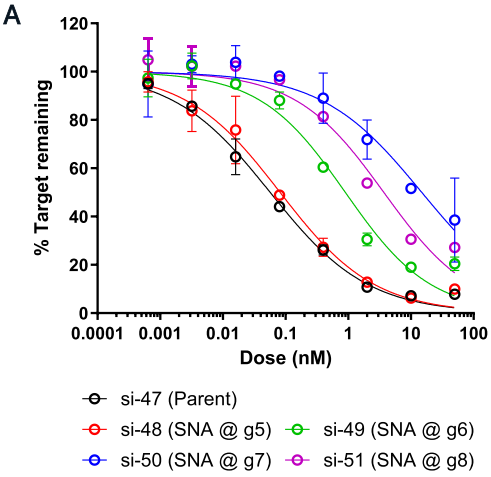

B

GalNAc-siRNA	Position of SNA Modification	On-Target IC_{50} (pM)	Off-Target IC_{50} (nM)	Off-/On-target ratio	Fold-change to parent
si-47	Parent	5.0	0.057	11	-
si-48	g5	2.6	0.082	32	2.9
si-49	g6	2.7	0.90	330	30
si-50	g7	2.0	15	7500	680
si-51	g8	4.4	3.7	840	76

IC_{50} values were calculated using GraphPad Prism and a fit of [GalNAc-siRNA] vs % Target remaining using a variable slope.

Figure 5. Activity of GalNAc–siRNAs targeting *Ttr* in (**A**) the dual-luciferase off-target reporter assay in COS-7 cells and (**B**) the corresponding on-target, off-target IC_{50} values, and relative ratios ($n = 4$).

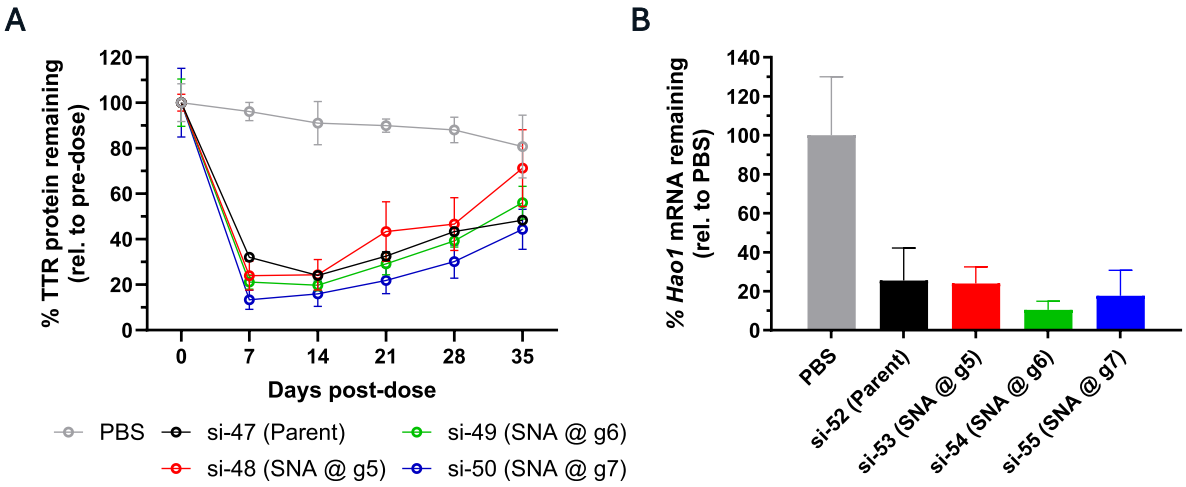

Figure 6. Evaluation of SNA-modified GalNAc–siRNA activity in C57BL/6 mice. (**A**) Serum TTR protein levels in mice ($n = 3$) after subcutaneous administration of a 0.5 mg/kg dose of the specified GalNAc–siRNA. (**B**) Knockdown of liver *Hao1* mRNA in mice ($n = 3$) normalized to PBS control after subcutaneous administration of a 1 mg/kg dose of the specified GalNAc–siRNA. Data for si-52 is representative of the average of four independent experiments; data for si-53 and si-55 is representative of the average of two independent experiments of $n = 3$ each.

We next assessed both off- and on-target activity of these SNA-modified GalNAc–siRNAs in two separate dual-luciferase reporters expressing four tandem repeats of the seed region (off-target) or the full complement to the guide strand (on-target). The on-target activity was maintained or slightly improved for each SNA-modified GalNAc–siRNA relative to the parent sequence (Fig. 5 and Supplementary Fig. S7). In three of the four positions tested (g6, g7, and g8), a variable increase in off-target IC_{50} value was observed, indicating a position-specific mitigation of off-targeting behavior (Fig. 5A). The presence of SNA in position g5 (si-48) maintained an almost identical level of miRNA-like off-target activity when compared to the parent sequence si-47. Relatively modest decreases in off-target behavior relative to the parent were observed when SNA was included in position g6 or g8 of si-49 and si-51, with increases in IC_{50} values of ~16- or ~65-fold, respectively (Fig. 5B). The greatest impact of SNA modification was observed when included at position g7 in si-50, with a relative off-target IC_{50} increase of ~260-fold over the parent si-47. The relative ratio of off- to on-target activity can provide a means by which to better assess the overall benefit of SNA substitution and allows for a comparison to what has previously been reported for GNA [21]. Interestingly, the effect of SNA substitution on off- to on-target ratio was not as robust as that reported for GNA, with a stronger position-specific effect and lower ratios than the range of ~200–12 000 reported for GNA. However, the relative fold change to the parent, which accounts for assay variability across individual experiments, showed that SNA at g7 demonstrated an ~680-fold improvement of off- to on-target ratio compared to an ~300-fold improvement with GNA at the same position. The strongest effect was observed with GNA at position g5 of this sequence, but that resulted in only ~380-fold improvement in off- to on-target ratio. It should be noted, however, that a direct comparison is challenging since the IC_{50} values for GNA-modified siRNAs in the dual-luciferase off-target reporter were defined as >50 nM because this was the highest dose tested in these assays, whereas SNA had well-defined

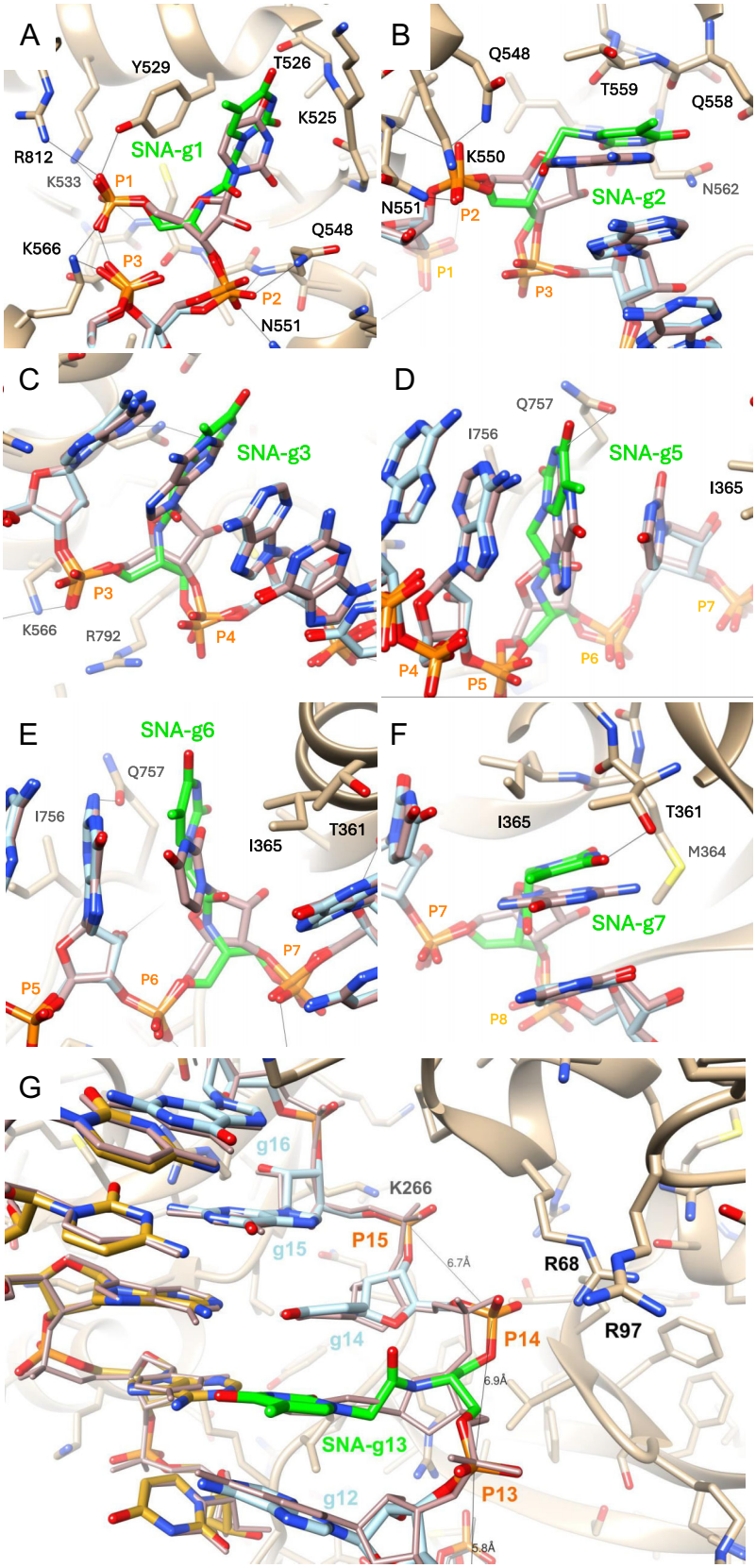

Figure 7. Modeling of SNA fit and interactions at various sites in the siRNA guide strand bound to Ago2 starting from the crystal structures of Ago2–RNA complexes (PDB ID 4f3t, panels (A–F); PDB ID 6n40, panel (G). (**A**) g1, (**B**) g2, (**C**) g3, (**D**) g5, (**E**) g6, (**F**) g7, and (**G**) g13. Ago2 in the energy-minimized complexes is shown in ribbon mode colored in tan with selected side chains displayed and labeled. Carbon atoms of the modeled guide strand are colored in light blue, except for those in SNA-T that are highlighted in green. In panel (G), carbon atoms of the modeled passenger strand are colored in goldenrod. Guide and passenger RNA strands observed in the crystal structures of Ago2 complexes are overlaid with carbon atoms colored in brown. H-bonds in the modeled complexes are drawn with thin black lines. In panel (G), selected P-P distances are drawn with thin solid lines.

IC_{50} values in both reporter assays. Head-to-head experiments across *in vitro* and *in vivo* models would allow for a more robust comparison of how effectively each modification can improve GalNAc–siRNA specificity and safety.

In vivo gene silencing of modified siRNA containing SNA modifications

We next evaluated the pharmacodynamics of RNAi-mediated silencing for three of the four SNA-modified GalNAc–siRNAs that were tested in the dual-luciferase reporter assays. After subcutaneous dosing of 0.5 mg/kg for each GalNAc–siRNA, TTR expression was monitored by protein ELISA of mouse serum over a period of 35 days (Fig. 6A). Administration of the parent si-47 led to a 76% reduction in circulating TTR protein with a nadir of ∼14 days. Interestingly, all tested GalNAc–siRNAs containing SNA demonstrated a similar or greater level of silencing at nadir, leading to 76%, 80%, and 84% target suppression for si-48, si-49, and si-50 modified at g5, g6, and g7, respectively. Moreover, the silencing duration was comparable for si-47, si-49, and si-50, but the activity with si-48, with SNA at position g5, showed a slightly faster recovery. A similar trend in activity and duration was observed for the same parent GalNAc–siRNA containing GNA at position g7, but not for those modified with GNA at position g5 or g6 where a statistically significant loss of potency and duration was observed [21].

To confirm the generalizability of these trends, we evaluated a second series of SNA-modified GalNAc–siRNAs targeting *Hao1* (hydroxyacid oxidase 1) in mice (Supplementary Table S7). We first confirmed a similar trend and magnitude of thermal destabilization due to SNA incorporation in position g5–g8 of the seed region (Supplementary Tables S7 and S8, and Supplementary Figs S5 and S6). The parent GalNAc–siRNA, si-52, or those modified with SNA at positions g5 (si-53), g6 (si-54), or g7 (si-55) were subcutaneously administered to mice at a dose of 1 mg/kg (Fig. 6B). The mice were subsequently sacrificed 7 days post-dose and mRNA expression quantified from liver. *Hao1* mRNA was suppressed by 75% after administration of the parent si-52. A similar trend emerged as in the *Ttr*-targeting series whereby all three SNA-modified GalNAc–siRNAs targeting *Hao1* demonstrated a robust level of silencing consistent with or exceeding that of the parent. *Hao1* expression was reduced by 76%, 90%, or 82% with si-53, si-54, or si-55 modified at g5, g6, or g7, respectively. This trend is again only partially consistent with that of GNA, where GalNAc–siRNAs modified at positions g6 or g7 with GNA showed robust silencing like that of the parent, but the modification of position g5 with GNA led to a reduced target silencing [21, 24].

To further understand the observed differences in activity between these SNA or GNA g5-modified GalNAc–siRNAs targeting *Hao1* in mice, we leveraged metabolite profiling via mass spectrometry from the livers of mice 7 days after dosing with si-52 or si-53 and compared with our previously reported data for the corresponding GNA-modified siRNA [22]. We chose this comparison since it was one of the most prominent examples where GNA modification led to an almost complete loss in activity in mice due to a strong metabolism of the guide strand. In line with the GNA-modified GalNAc–siRNA, we identified metabolism of the guide strand nucleotides 5′- of the SNA-C incorporation which accounted for 65% of the detected guide strand species in the liver (Supplementary Table S9 and Supplementary Fig. S8). The other 35% of the detected guide strand consisted of the full-length and 3′-N-1 metabolites, which are both considered to be active species. The identified metabolites of parent si-52 guide strand detected in the liver consisted of 100% of the active species. In contrast, only 13% of the active species with the g5-GNA-modified GalNAc–siRNA were detected in mouse liver under the same conditions [22]. This less significant metabolism of the SNA-containing siRNA and the concomitant ∼3-fold increase in active species likely accounts for the differences in activity observed in mice for GNA and SNA modification at g5 of this *Hao1*-targeted GalNAc–siRNA. The observed disparity in activity, duration, and metabolism between SNA- and GNA-modified GalNAc–siRNAs would suggest that SNA is better tolerated in some of the tested positions relative to GNA and warrants further investigation.

Discussion

RNAi therapeutics make use of chemical modifications to improve their drug-like properties, such as nuclease resistance, reduction of immunostimulatory effects, optimal PK/PD profiles, targeted delivery, and on-target specificity. This has prompted significant efforts toward the investigation of various noncanonical modifications. Previous reports have detailed the intriguing utility of SNA nucleotides for their resistance to exonucleases, to reduce passenger-strand-mediated off-target effects of siRNAs, to efficiently modulate splice-switching of a mouse dystrophin mRNA transcript, and to improve the duration and safety of gapmer ASOs. In this report, we studied the biophysical and biological properties of SNA-modified siRNAs and compared these findings to those results previously reported for another acyclic nucleic acid analog, GNA. We utilized X-ray crystallography to rationalize the behavior of SNA nucleotides in RNA duplexes and subsequently demonstrated the potential utility for SNA modification in the development of more specific RNAi therapeutics through the mitigation of seed-mediated, miRNA-like suppression of off-target mRNAs.

The decreased thermal stability of RNA or GalNAc–siRNA duplexes modified with SNA was in line with previous reports on SNA and was comparable to the level of thermal destabilization afforded by GNA modification of the same sequences. Given the flexible nature of the SNA backbone, and the structural distortions introduced through SNA modification that were observed in the RNA dodecamer crystal structure, it is perhaps unsurprising to observe this level of duplex thermal destabilization. SNA differs in one key aspect in its comparison to GNA; that is, unlike GNA, SNA presumably does not suffer from inefficient base pairing of C- and G-nucleotides to the complementary nucleotide, resulting in less-significant duplex thermal destabilization, and hypothetically improved metabolic stability when incorporated into an siRNA. The trend whereby the modification of C- or G-nucleotides in the GalNAc–siRNA with acyclic monomers such as SNA or GNA results in, on average, significantly more thermal destabilization relative to the same modification of A- or U-nucleotides is intriguing and requires further investigation. A potential explanation for this stability trend observed with SNA:RNA pairing could be that the shift in the SNA nucleobase relative to native RNA (Fig. 3C) is likely to more substantially affect the pairing geometry and formation of three optimal H-bonds

in RNA:SNA G:C (C:G) base pairs compared to the formation of two optimal H-bonds in RNA:SNA A:T (U:A) pairs.

SNA modification was tolerated at multiple positions across both strands of the tested GalNAc–siRNA, especially when placed in positions g5–g8 of the seed region. Although SNA modification of positions g6–g8 in the model GalNAc–siRNA demonstrated the ability to mitigate miRNA-like off-target behavior, the strongest effect was observed when SNA was placed at position g7. Given the similar level of thermal destabilization caused by SNA modification of g6 or g7 in this sequence (−6.5°C or −4.0°C, respectively), but substantially different levels of effect on the mitigation of miRNA-like off-targets (∼30-fold or ∼680-fold increase in off- to on-target ratio relative to parent, respectively), it is reasonable to hypothesize that thermal destabilization of the seed region alone is not sufficient to suppress these seed-mediated off-target effects. These findings mimic that of our previous report with GNA and 2′-5′-RNA linkages, whereby position of the modification rather than level of thermal destabilization appeared to be a key factor in determining the extent of off-target mitigation. Another recent report using phosphonate linkages between g6 and g7 for the suppression of off-targets further supports this hypothesis; similar to what we have reported for GNA, 2′,5′-RNA, and now SNA, T_M differences alone were not effective in predicting the ability of alkyl phosphonate linkages to mitigate off-targets, but rather more complex factors such as guide–Ago2 interactions and conformational changes were considered to be more impactful [17]. As we have shown here, SNA introduces a longer P-P distance at the site of incorporation, like 2′-5′-RNA, and potentially explains the similarity in behavior toward improving specificity where both modifications were most effective when incorporated at g7 [21, 53–55]. Encouragingly, the pharmacodynamic activity of two different GalNAc–siRNAs modified with SNA at position g5, g6, or g7 translated effectively into mice, further supporting the utility of SNA as a modification that can improve siRNA specificity while maintaining robust on-target activity.

To gain insight into the regiospecific changes in potency observed in the walk of a single SNA nucleotide along a GalNAc–siRNA guide strand, we modeled Ago2 complexes with a guide strand featuring a single SNA residue at selected sites (Fig. 7). Given that the incorporation of SNA-T into an RNA duplex was accompanied by significant conformational changes both at the global (helical rise, base-pair inclination, major groove width) and local level (intra-strand P-P distance, duplex diameter, unwinding), it is perhaps surprising that SNA is quite well tolerated at many positions of the guide strand, with comparable activities to that of the parent si-1. At position g1, SNA-T fits quite well and the nucleobase maintains stacking with Y529 without causing close contacts to main chain atoms of K525 and T526 (Fig. 7A). The orientations and positions of both 5′-phosphates P1 and P2 are very similar in the Ago2 crystal structure and the modeled complex with SNA-T at g1. Conversely, at position g2, the SNA-T thymine and adenine at g3 are unstacked and the presence of the SNA residue at that site creates unfavorable contacts with side and main chain atoms of Q558 and T559 that are part of an α-helix (Fig. 7B). This helix can move just slightly but is unable to accommodate the longer linker between SNA backbone and base compared to a ribonucleotide. The changes at the structural level seen in the model are in line with the significant reduction in activity observed for SNA at g2. The excellent fit of SNA at position g3 correlates well with the activity of the modified siRNA that matches that of the parent strand (Fig. 7C). A similar picture emerges for SNA at positions g5 and g6. SNA at position g5 maintains stacking with neighboring bases and an H-bond between the base and the side chain of Q757 (Fig. 7D). The structural model also supports the notion that SNA can mimic a ribonucleotide at g6, the site of a kink in guide siRNA that features the side chain of I365 inserted between the bases of g6 and g7 nucleotides [48, 11, 56].

However, incorporating SNA at position g7 creates a suboptimal fit compared to g5 or g6 as the SNA nucleotide there does not maintain stacking with the g8 nucleotide (Fig. 7F). The loss of stacking is due to the keto oxygen of SNA pushing against the g8 nucleobase and thereby preventing the g7 base from assuming an ideal 3.4 Å spacing. Because the side chain of I365 stacks on the g7 base in the parent Ago2 complex, the isoleucine is pushed up alongside the g7 SNA base. The altered position of the g7 base in the SNA-modified guide strand allows for formation of a H-bond between O4 of SNA-T and Oγ of T361. Both I365 and T361 are associated with the kink in the guide strand between residues g6 and g7. GNA with its shorter backbone perfectly mimics the 5.5 Å distance between adjacent phosphates in the parent RNA structure at the site of the kink. SNA's backbone cannot contract to <6 Å between adjacent phosphates at g7 but maintains the kink by splaying apart the g6 and g8 nucleobases with the assistance of its keto group. This is somewhat reminiscent of the situation with the gem-2′-F/Me modification at g7 where the axial methyl group pushes against the g8 base [25]. Interestingly, the thermal destabilization at the g6 and g7 positions caused by SNA are quite similar and both the *in vitro* and *in vivo* data show robust activity for SNA at g6 and g7 (Figs 4–6). Thus, SNA's ability to maintain a strong kink in the guide strand at g7 through control of the relative orientation of the g6 and g8 bases while maintaining the interaction of the g7 nucleobase with I365 and T361 fundamentally distinguishes SNA incorporated at g6 and g7, likely providing an explanation for the drastically different off-target mitigation observed with SNA modification at the two sites (Fig. 5).

The gain in activity triggered by SNA modification at g13 is quite striking (Fig. 4B). To better understand this effect, we turned to the crystal structure of a guide-passenger strand duplex with a well-defined supplementary region in complex with human Ago2 (PDB ID 6n4o; [49]). The structure allows visualization of the spatial relationship between the g2–g8 seed region and the g13–g16 supplementary region. The latter stretch is fully paired to the passenger or target strand and, interestingly, the P-P distances for g12–g13, g13–g14, and g14–g15 are 5.5, 6.8, and 5.7 Å, respectively. The observed distances for SNA inside double helical RNA of 6.5 and 6.6 Å (Fig. 3A) match the observed, slightly stretched g13 backbone in the 6n4o crystal structure with Ago2. Furthermore, the virtual absence of a helical twist between the bases of g12 and g13 in the complex crystal structure is noteworthy as this also matches this property of SNA inside RNA in our crystal structure, i.e. the twist there is just slightly negative (Fig. 3B). Using the structure of the Ago2 complex with PDB ID 6n4o, we built a model with SNA-T at g13 opposite A using the UCSF Chimera suite [50] and energy-minimized the modified complex with Amber [51]. A comparison between the model with SNA-T at position g13 with the crystal structure of the parent complex is depicted in Fig. 7G. The overlay shows a

good overall fit of the supplementary regions and that the wider SNA residue can be quite well accommodated in terms of Watson–Crick pairing. Finally, SNA is well tolerated at the 3′-terminal end of the guide strand that is bound to the Ago2 PAZ domain. Indeed, the models with SNA at positions g22 (Supplementary Fig. S9A) and g23 (Supplementary Fig. S9B) demonstrate a relatively good fit in both cases.

Continued progress toward novel siRNA chemical modifications will provide additional opportunities to improve the performance of therapeutic siRNAs, as well as to improve our understanding of RNAi mechanism. This work highlights a position-specific utility of SNA toward improving the on-target specificity of siRNAs, which can demonstrate miRNA-like effects through seed-pairing to undesired off-targets. Since our prior work has demonstrated the connection between off-target activity and safety, SNA can now be added to the list of modifications that have the potential to improve the safety and therapeutic index of siRNAs, warranting further preclinical investigation of this modification for the development of potent and safe therapeutic siRNAs. Future directions include the additional determination of sequence- and position-specific effects of SNA on off-target mitigation, a broader characterization of the metabolite profiles of SNA-modified siRNAs, and the potential to leverage a synergistic effect by incorporating multiple SNA nucleotides into siRNAs.

Acknowledgements

The authors would like to thank all members of the RNA synthesis, *in vitro* screening, and animal care facilities who helped support the execution of these studies. This research used resources of the Advanced Photon Source and the Life Sciences Collaborative Access Team (LS-CAT, sector 21) of which Vanderbilt University is a member.

Author contributions: Tyler Chickering (Data curation [equal], Formal analysis [equal], Methodology [supporting], Writing—original draft [supporting], Writing—review & editing [supporting]), Joel M. Harp (Formal analysis [supporting], Methodology [supporting], Resources [supporting]), Yongfeng Jiang (Data curation [supporting], Formal analysis [supporting], Methodology [supporting], Resources [supporting]), June Qin (Data curation [supporting], Formal analysis [supporting], Resources [supporting]), Guo He (Data curation [supporting], Formal analysis [supporting], Resources [supporting]), Sarah Hyde (Data curation [supporting], Formal analysis [supporting], Resources [supporting]), Audrey Ihlefeld (Data curation [supporting], Formal analysis [supporting], Resources [supporting]), Maja M. Janas (Conceptualization [supporting], Formal analysis [equal], Supervision [supporting], Writing—review & editing [supporting]), Derek O'Flaherty (Formal analysis [supporting], Writing—original draft [supporting]), Sally Schofield (Data curation [supporting], Formal analysis [supporting], Resources [supporting]), John Szeto (Data curation [supporting], Formal analysis [supporting], Resources [supporting]), Christopher Theile (Formal analysis [supporting], Resources [supporting]), Vasant Jadhav (Conceptualization [supporting], Formal analysis [supporting], Resources [supporting], Supervision [equal]), Klaus B. Charissé (Formal analysis [supporting], Resources [supporting], Supervision [supporting]), Martin A. Maier (Conceptualization [equal], Formal analysis [supporting], Resources [supporting], Supervision [equal]), Muthiah Manoharan (Conceptualization [equal], Formal analysis [equal], Supervision [equal], Writing—original draft [equal], Writing—review & editing [equal]), Martin Egli (Formal analysis [lead], Methodology [equal], Resources [equal], Writing—original draft [lead], Writing—review & editing [lead]), and Mark K. Schlegel (Conceptualization [equal], Data curation [lead], Formal analysis [lead], Project administration [lead], Resources [lead], Supervision [lead], Writing—original draft [lead], Writing—review & editing [lead]).

Supplementary data

Supplementary data is available at NAR online.

Conflict of interest

Apart from Martin Egli and Joel M. Harp, all authors were employees of Alnylam Pharmaceuticals at the time this work was conducted.

Funding

This work, including for open access publishing, was supported by Alnylam Pharmaceuticals.

Data availability

Atomic coordinates and structure factors for the reported crystal structure have been deposited with the Protein Data Bank under accession number 9O47.

References

1. Meister G, Landthaler M, Patkaniowska A *et al.* Human Argonaute2 mediates RNA cleavage targeted by miRNAs and siRNAs. *Mol Cell* 2004;15:185–97. https://doi.org/10.1016/j.molcel.2004.07.007
2. Fire A, Xu S, Montgomery MK *et al.* Potent and specific genetic interference by double-stranded RNA in Caenorhabditis elegans. *Nature* 1998;391:806–11. https://doi.org/10.1038/35888
3. The eight approved siRNA therapeutics include Onpattro (Patisiran), Givlaari (Givosiran), Oxlumo (Lumasiran), Leqvio (Inclisiran), Amvuttra (Vutrisiran), Rivfloza (Nedosiran), Qfitlia (Fitusiran), and Redemplo (Plozasiran).
4. Nair JK, Willoughby JLS, Chan A *et al.* Multivalent NAcetylgalactosamine-conjugated siRNA localizes in hepatocytes and elicits robust RNAi-mediated gene silencing. *J Am Chem Soc* 2014;136:16958–61. https://doi.org/10.1021/ja505986a
5. Prakash TP, Graham MJ, Yu J *et al.* Targeted delivery of antisense oligonucleotides to hepatocytes using triantennary N-acetyl galactosamine improves potency 10-fold in mice. *Nucleic Acids Res* 2014;42:8796–807. https://doi.org/10.1093/nar/gku531
6. Zimmermann TS, Karsten V, Chan A *et al.* Clinical proof of concept for a novel hepatocyte-targeting GalNAc–siRNA conjugate. *Mol Ther* 2017;25:71–8. https://doi.org/10.1016/j.ymthe.2016.10.019
7. Nair JK, Attarwala H, Sehgal A *et al.* Impact of enhanced metabolic stability on pharmacokinetics and pharmacodynamics of GalNAc–siRNA conjugates. *Nucleic Acids Res* 2017;45:10969–77. https://doi.org/10.1093/nar/gkx818
8. Foster DJ, Brown CR, Shaikh S *et al.* Advanced siRNA designs further improve in vivo performance of GalNAc–siRNA conjugates. *Mol Ther* 2018;26:708–17. https://doi.org/10.1016/j.ymthe.2017.12.021
9. Brown KM, Nair JK, Janas MM *et al.* Expanding RNAi therapeutics to extrahepatic tissues with lipophilic conjugates. *Nat*

Biotechnol 2022;40:1500–8. https://doi.org/10.1038/s41587-022-01334-x
10. Jayaraman M, Ansell SM, Mui BL *et al.* Maximizing the potency of siRNA lipid nanoparticles for hepatic gene silencing *in vivo*. *Angew Chem Int Ed* 2012;51:8529–33. https://doi.org/10.1002/anie.201203263
11. Schirle NT, Sheu-Gruttadauria J, MacRae IJ. Structural basis for microRNA targeting. *Science* 2014;346:608–13. https://doi.org/10.1126/science.1258040
12. Bramsen JB, Pakula MM, Hansen TB *et al.* A screen of chemical modifications identifies position-specific modification by UNA to most potently reduce siRNA off-target effects. *Nucleic Acids Res* 2010;38:5761–73. https://doi.org/10.1093/nar/gkq341
13. Lee H-S, Seok H, Lee DH. *et al.* Abasic pivot substitution harnesses target specificity of RNA interference. *Nat Commun* 2015;6:10154. https://doi.org/10.1038/ncomms10154
14. Pal C, Richter M, Harasgama J *et al.* Amide internucleoside linkages suppress the microRNA-like off-target activity of short interfering RNA. *ACS Chem Biol* 2025;20:522–8. https://doi.org/10.1021/acschembio.4c00824
15. Richter M, Viel JA, Kotikam V *et al.* Amide modifications in the seed region of the guide strand improve the on-target specificity of short interfering RNA. *ACS Chem Biol* 2023;18:7–11. https://doi.org/10.1021/acschembio.2c00769
16. Vaish N, Chen F, Seth S *et al.* Improved specificity of gene silencing by siRNAs containing unlocked nucleobase analogs. *Nucleic Acids Res* 2011;39:1823–32. https://doi.org/10.1093/nar/gkq961
17. Nikan M, Li Q, Tanowitz M *et al.* Single alkyl phosphonate modification of the siRNA backbone in the seed region enhances specificity and therapeutic profile. *Nucleic Acids Res* 2025;53:gkaf692. https://doi.org/10.1093/nar/gkaf692
18. Nomura K, An S, Kobayashi Y *et al.* Synthesis of 2′-formamidonucleoside phosphoramidites for suppressing the seed-based off-target effects of siRNAs. *Nucleic Acids Res* 2024;52:10754–74. https://doi.org/10.1093/nar/gkae741
19. Laursen MB, Pakula MM, Gao S *et al.* Utilization of unlocked nucleic acid (UNA) to enhance siRNA performance *in vitro* and *in vivo*. *Mol Biosyst* 2010;6:862–70. https://doi.org/10.1039/B918869J
20. Schlegel MK, Foster DJ, Kel'in AV *et al.* Chirality dependent potency enhancement and structural impact of glycol nucleic acid modification on siRNA. *J Am Chem Soc* 2017;139:8537–46. https://doi.org/10.1021/jacs.7b02694
21. Schlegel MK, Janas MM, Jiang Y *et al.* From bench to bedside: improving the clinical safety of GalNAc–siRNA conjugates using seed-pairing destabilization. *Nucleic Acids Res* 2022;50:6656–70. https://doi.org/10.1093/nar/gkac539
22. Schlegel MK, Matsuda S, Brown CR *et al.* Overcoming GNA/RNA base-pairing limitations using isonucleotides improves the pharmacodynamic activity of ESC+ GalNAc–siRNAs. *Nucleic Acids Res* 2021;49:10851–67. https://doi.org/10.1093/nar/gkab916
23. Matsuda S, Bala S, Liao J-Y *et al.* Shorter is better: the α(l)Threofuranosyl nucleic acid modification improves stability, potency, safety, and Ago2 binding and mitigates off-target effects of small interfering RNAs. *J Am Chem Soc* 2023;145:19691–706. https://doi.org/10.1021/jacs.3c04744
24. Janas MM, Schlegel MK, Harbison CE *et al.* Selection of GalNAc-conjugated siRNAs with limited off-target-driven rat hepatotoxicity. *Nat Commun* 2018;9:723. https://doi.org/10.1038/s41467-018-02989-4
25. Guenther DC, Mori S, Matsuda S *et al.* Role of a "Magic" methyl: 2′-deoxy-2′-α-F-2′-βCmethyl pyrimidine nucleotides modulate RNA interference activity through synergy with 5′-phosphate mimics and mitigation of off-target effects. *J Am Chem Soc* 2022;144:14517–34. https://doi.org/10.1021/jacs.2c01679
26. Gane E, Lim Y-S, Kim JB *et al.* Evaluation of RNAi therapeutics VIR-2218 and ALN-HBV for chronic hepatitis B: results from randomized clinical trials. *J Hepatol* 2023;79:924–32. https://doi.org/10.1016/j.jhep.2023.05.023
27. Ramasamy KS, Seifert W. Amino acid nucleic acids: synthesis and hybridization properties of a novel class of antisense oligonucleotides. *Bioorg Med Chem Lett* 1996;6:1799–804. https://doi.org/10.1016/0960-894X(96)00320-4
28. Benhida R, Devys M, Fourrey J-L *et al.* Incorporation of serinol derived acyclic nucleoside analogues into oligonucleotides: influence on duplex and triplex formation. *Tetrahedron Lett* 1998;39:6167–70. https://doi.org/10.1016/S0040-4039(98)01268-4
29. Kashida H, Murayama K, Toda T *et al.* Control of the chirality and helicity of oligomers of serinol nucleic acid (SNA) by sequence design. *Angew Chem Int Ed* 2011;50:1285–8. https://doi.org/10.1002/anie.201006498
30. Sharma AK, Kumar P, Gupta KC. Synthesis and hybridization properties of sugar-modified oligonucleotides. *Helvetica Chim Acta* 2001;84:3643–9.
31. Asanuma H, Toda T, Murayama K *et al.* Unexpectedly stable artificial duplex from flexible acyclic threoninol. *J Am Chem Soc* 2010;132:14702–3. https://doi.org/10.1021/ja105539u
32. Murayama K, Kashida H, Asanuma H. *Acyclic* L-threoninol nucleic acid (L-*a*TNA) with suitable structural rigidity cross-pairs with DNA and RNA. *Chem Commun* 2015;51:6500–3. https://doi.org/10.1039/C4CC09244A
33. Kamiya Y, Satoh T, Kodama A *et al.* Intrastrand backbone-nucleobase interactions stabilize unwound right-handed helical structures of heteroduplexes of L-*a*TNA/RNA and SNA/RNA. *Commun Chem* 2020;3:156. https://doi.org/10.1038/s42004-020-00400-2
34. Tsuboi T, Hattori K, Ishimoto T *et al.* In vivo efficacy and safety of systemically administered serinol nucleic acid-modified antisense oligonucleotides in mouse kidney. *Mol Ther Nucleic Acids* 2025;36:102387. https://doi.org/10.1016/j.omtn.2024.102387
35. Kamiya Y, Takeyama Y, Mizuno T *et al.* Investigation of strand-selective interaction of SNA-modified siRNA with AGO2-MID. *Int J Mol Sci* 2020;21:5218. https://doi.org/10.3390/ijms21155218
36. Le BT, Murayama K, Shabanpoor F *et al.* Antisense oligonucleotide modified with serinol nucleic acid (SNA) induces exon skipping in mdx myotubes. *RSC Adv* 2017;7:34049–52. https://doi.org/10.1039/C7RA06091B
37. Kamiya Y, Takai J, Ito H *et al.* Enhancement of stability and activity of siRNA by terminal substitution with serinol nucleic acid (SNA). *ChemBioChem* 2014;15:2549–55. https://doi.org/10.1002/cbic.201402369
38. Alagia A, Jorge AF, Aviñó A *et al.* Exploring PAZ/3′-overhang interaction to improve siRNA specificity. A combined experimental and modeling study. *Chem Sci* 2018;9:2074–86. https://doi.org/10.1039/C8SC00010G
39. Alagia A, Terrazas M, Eritja R. Modulation of the RNA interference activity using central mismatched siRNAs and *acyclic* threoninol nucleic acids (*a*TNA) units. *Molecules* 2015;20:7602–19. https://doi.org/10.3390/molecules20057602
40. Alagia A, Terrazas M, Eritja R. RNA/aTNA chimeras: RNAi effects and nucleases resistance of single and double stranded RNAs. *Molecules* 2014;19:17872–96. https://doi.org/10.3390/molecules191117872
41. Winter G. xia2: an expert system for macromolecular crystallography data reduction. *J Appl Crystallogr* 2010;43:186–90. https://doi.org/10.1107/S0021889809045701
42. Winter G, Waterman DG, Parkhurst JM *et al.* DIALS: implementation and evaluation of a new integration package. *Acta Crystallogr D Struct Biol* 2018;74:85–97. https://doi.org/10.1107/S2059798317017235
43. Pape T, Schneider TR. HKL2MAP: a graphical user interface for macromolecular phasing with SHELX programs. *J Appl Crystallogr* 2004;37:843–4. https://doi.org/10.1107/S0021889804018047

44. Schneider TR, Sheldrick GM. Substructure solution with SHELXD. *Acta Crystallogr D Biol Crystallogr* 2002;58:1772–9. https://doi.org/10.1107/S0907444902011678
45. Sheldrick GM. Macromolecular phasing with SHELXE. *Z für Krist - Cryst Mater* 2002;217:644–50. https://doi.org/10.1524/zkri.217.12.644.20662
46. Emsley P, Lohkamp B, Scott WG *et al.* Features and development of Coot. *Acta Crystallogr D Biol Crystallogr* 2010;66:486–501. https://doi.org/10.1107/S0907444910007493
47. Liebschner D, Afonine PV, Baker ML *et al.* Macromolecular structure determination using X-rays, neutrons and electrons: recent developments in Phenix. *Acta Crystallogr D Struct Biol* 2019;75:861–77. https://doi.org/10.1107/S2059798319011471
48. Elkayam E, Kuhn C-D, Tocilj A *et al.* The structure of human argonaute-2 in complex with miR-20a. *Cell* 2012;150:100–10. https://doi.org/10.1016/j.cell.2012.05.017
49. Sheu-Gruttadauria J, Xiao Y, Gebert LF *et al.* Beyond the seed: structural basis for supplementary microRNA targeting by human Argonaute2. *EMBO J* 2019;38:EMBJ2018101153. https://doi.org/10.15252/embj.2018101153
50. Pettersen EF, Goddard TD, Huang CC *et al.* UCSF Chimera—a visualization system for exploratory research and analysis. *J Comput Chem* 2004;25:1605–12. https://doi.org/10.1002/jcc.20084
51. Case DA, Cheatham TE III, Darden T *et al.* The AMBER biomolecular simulation programs. *J Comput Chem* 2005;26:1668–88. https://doi.org/10.1002/jcc.20290
52. Mohamed AA, Wang PY, Bartel DP *et al.* The structural basis for RNA slicing by human Argonaute2. *Cell Rep* 2025;44:115166. https://doi.org/10.1016/j.celrep.2024.115166
53. Lalitha V, Yathindra N. Even nucleic acids with 2′,5′-linkages facilitate duplexes and structural polymorphism: prospects of 2′,5′-oligonucleotides as antigene/antisense tool in gene regulation. *Curr Sci* 1995;68:68.
54. Sheng J, Li L, Engelhart AE *et al.* Structural insights into the effects of 2′–5′ linkages on the RNA duplex. *Proc Natl Acad Sci USA* 2014;111:3050–5. https://doi.org/10.1073/pnas.1317799111
55. Habibian M, Harikrishna S, Fakhoury J *et al.* Effect of 2′–5′/3′–5′ phosphodiester linkage heterogeneity on RNA interference. *Nucleic Acids Res* 2020;48:4643–57. https://doi.org/10.1093/nar/gkaa222
56. Schirle NT, MacRae IJ. The crystal structure of human Argonaute2. *Science* 2012;336:1037–40. https://doi.org/10.1126/science.1221551

Received: November 25, 2025. **Revised:** February 25, 2026. **Accepted:** March 22, 2026